Local Structure Effects on Pressure Drop in Slender Fixed Beds of Spheres

Steffen Flaischlen[1,2,*], Martin Kutscherauer[1,3], and Gregor D. Wehinger[1,2]

DOI: 10.1002/cite.202000171

Supporting Information available online

Dedicated to Prof. Dr.-Ing. Matthias Kraume on the occasion of his 65th birthday

For slender fixed beds, the void fraction and flow properties are complex topics. Different factors can influence the local bed structure. For statistical analysis, 2800 fixed beds have been generated and the impact of friction factor and reactor-to-particle diameter ratio on the distribution has been shown. With particle-resolved computational fluid dynamics, all local structure effects are taken into account for the flow simulations. Pressure drop measurements and simulations showed that these effects can lead to areas with low flow resistance, leading to overestimated pressure drop by typical correlations up to 85 %.

Keywords: Computational fluid dynamics, Fixed bed reactor, Pressure drop, Rigid body approach, Synthetic fixed beds

Received: July 31, 2020; *revised:* November 18, 2020; *accepted:* November 20, 2020

1 Introduction

The fixed bed reactor is a type of reactor commonly used in chemical process engineering. A characterization of fixed beds can be carried out by both structural properties (e.g., void fraction) and flow properties (e.g., pressure drop). An important parameter of fixed beds is the void fraction, i.e., the ratio between open and solid volume. Recent research has shown that the filling methods and material properties of particles have a large influence on the mean bed void fraction [1–4]. For slender fixed beds, for which the ratio between reactor diameter and particle diameter D/d_p reaches values of smaller 10, the confining wall influences the bed structure, which leads to zones of high and low void fraction in the radial direction [5, 6]. Various correlations for the void fraction prediction can be found in the literature [7–11]. All of which are based on different data sets and thus lead to different values, especially for $D/d_p < 10$. A comparison between calculated mean bed void fractions depending on the reactor-to particle diameter ratio shows large differences for slender fixed beds [1]. According to recent work, it appears that the void fraction cannot be calculated as a simple monotonically decreasing function with D/d_p. Bufe and Brenner [12] showed with a theoretical approach a fluctuating profile of the void fraction over D/d_p. This is the result of the extra free space between the particles when D/d_p is not an integer. In addition, statistical investigations seem to be important for the interpretation of the stochastic bed generation process. Seckendorff et al. [1] showed different resulting void fractions of fixed beds using the same particle size, material and filling method. The pressure drop is an important process parameter as a representative value for the bed structure and the flow properties. Hence, several correlations, are available in literature [13]. All of them are mainly dependent on the mean bed void fraction (e.g., Ergun equation), while some of them also show a wall correction term for slender beds (e.g., Eisfeld-Schnitzlein equation) [13–15]. This main dependence on the void fraction simplifies the prediction of the pressure drop, especially for a slender fixed bed with a strong influence of the local structure. Small changes in the void fraction lead to much higher differences in pressure drop [1]. As an alternative, the use of computational fluid dynamics

[1]Steffen Flaischlen, Martin Kutscherauer,
Prof. Dr.-Ing. Gregor D. Wehinger
flaischlen@icvt.tu-clausthal.de
Clausthal University of Technology, Institute of Chemical and Electrochemical Process Engineering, Leibnizstraße 17, 38678 Clausthal-Zellerfeld, Germany.

[2]Steffen Flaischlen, Prof. Dr.-Ing. Gregor D. Wehinger
Clausthal University of Technology, Research Center Energy Storage Technologies (EST), Am Stollen 19A, 38640 Goslar, Germany.

[3]Martin Kutscherauer
Clariant AG, Waldheimer Straße 15, 83052 Bruckmühl, Germany.

(CFD) to calculate transport phenomena in fixed bed reactors seems to be promising. In contrast to homogeneous and heterogeneous reactor models, which require simplified assumptions and closure correlations, particle-resolved CFD simulations account for the local bed structure [16, 17]. For this purpose, the fixed bed is generated with an upstream synthetic packing generation. The most commonly used approaches are the discrete element method (DEM) and the rigid body approach (RBA) [17–20], which can take both the material properties and the filling method into account. In order to generate a synthetic bed representing an experimental fixed bed, the material properties (e.g., friction factor, etc.) can, therefore, be used as an adjustment factor [4].

In this work, experimental void fractions for slender beds made of spheres (D/d_p = 1.51, 2.68, 3.02) with synthetically generated fixed beds were compared using the RBA. Due to the randomness of the filling process, the resulting void fraction is different for each generated fixed bed having comparable overall properties, which hence leads to a statistical distribution. With the help of statistical analysis, it is possible to compare void fraction distributions of synthetically generated fixed beds with those of experimentally generated beds. The RBA that best represents the experimental fixed bed structure is then used as the input geometry of the subsequent particle-resolved CFD simulations. As an example of influence of local structure on transport phenomena, the pressure drop is investigated. For this purpose, CFD simulations are performed and compared with experimental data. An advantage of particle-resolved CFD is the independence from closure correlations. This means, the local structure of the fixed bed in the CFD simulation directly influences the resulting pressure drop. Furthermore, typical pressure drop correlations are used to study whether a given correlation can reflect the effects of a local structure.

2 Methods

2.1 Experimental Setup

The experimental setup (Fig. 1) consists of a reactor tube with a diameter D of 24.14 mm and a length of 600 mm that is filled with different particles. Two pressure sensors (Swagelok Company, Ohio, USA model: PTI-S-AA2.5-11AQ) located at the top and bottom of the fixed bed measured the inlet and outlet pressure. The top pressure sensor is used to calculate the inlet velocity (depending on the standard volume flow rate, temperature, and pressure). In combination with the bottom pressure sensor, the pressure drop over the fixed bed can be determined.

Normal volume flow rates of nitrogen from 2 to 60 $L_N\,min^{-1}$ are achieved using a mass flow controller (MFC, Bronkhorst High-Tech B.V. AK Ruurlo, Netherlands (Model: F-202AV-M10-AGD-55-V). The pressure drop over the experimental fixed beds was measured with a head

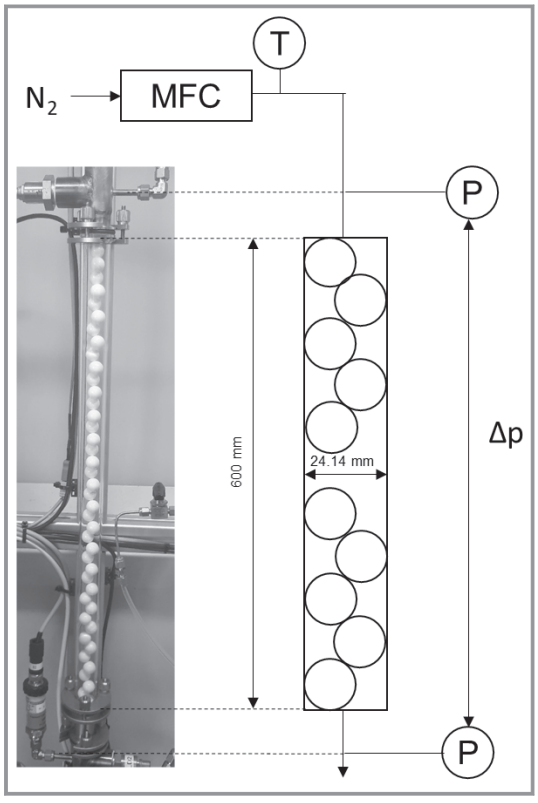

Figure 1. Pressure drop measurement setup.

pressure range from 950 to 1400 mbar, depending on the normal volume flow rate. The reactor was filled manually by dropping single particles, thus reflecting the used filling method for the synthetic fixed bed generation. By counting the particles in the tube, the void fraction ε was calculated with Eq. (1) from the particle diameter d_p, filling height H, reactor diameter D, and particle count N.

$$\varepsilon = 1 - \frac{2Nd_p^3}{3D^2H} \tag{1}$$

2.2 Numerical Setup

A fixed bed geometry, i.e., the packed bed structure, is required for both the calculation of the void fraction and the geometry input for consecutive CFD simulations. The workflow is based on the previous work of Partopour and Dixon [18] and Flaischlen and Wehinger [19] using the open source software Blender. For further information about the RBA see, e.g., [18, 19, 21]. Due to varying starting positions of each filled particle in the experiments, the particles in the simulation were injected with an initial velocity of zero at a random location within a defined space domain above the tube opening. The parameters, which were used for the synthetic fixed bed generation with RBA, are summarized in Tab. 1.

Table 1. Parameters for synthetic packed bed generation simulations.

Parameter	Value
Filling rate [mm³/Blender time frame]	8.94
Blender restitution coefficient C_{Res} [–]	0.818
Blender friction coefficient C_{Fric} [–]	0.001–0.9
Steps per second [s^{-1}]	200
Solver iterations [–]	200

The synthetic fixed bed is imported as a CAD geometry into the CFD software Simcenter STAR-CCM+ 2020.01 from Siemens for discretization (meshing) and particle-resolved CFD simulations. The particle-particle contacts were modified with the local caps method [22]. Thereby, the change of the bed structure is small, while the local flattening of the contact points and the insertion of fluid volume cells makes the solution numerically stable [23]. The CFD simulations presented here are based on the conservation of mass and momentum in three dimensions. The details of the modeling can be found in the general literature (see, e.g., [17]). The conservation of mass reads:

$$\nabla \cdot (\rho \mathbf{v}) = 0 \tag{2}$$

With the fluid density ρ and the velocity vector $\mathbf{v}$. The momentum conservation written with the stress tensor $\mathbf{T}$ reads:

$$\nabla \cdot (\rho \mathbf{v}\mathbf{v}) = \nabla \mathbf{T} \tag{3}$$

$$\mathbf{T} = -\left(p + \frac{2}{3}\mu \nabla \cdot \mathbf{v}\right)\mathbf{I} + 2\mu \mathbf{D} \tag{4}$$

The stress tensor is formulated with the gas dynamic viscosity μ, the unit tensor $\mathbf{I}$ the pressure p, and the deformation tensor $\mathbf{D}$, which reads:

$$\mathbf{D} = \frac{1}{2}\left[\nabla \mathbf{v} + (\nabla \mathbf{v})^{\mathbf{T}}\right] \tag{5}$$

The simulations were performed using a velocity inlet and a pressure outlet with an outlet pressure of 1 atm. The gas density was set to a constant value, depending on the inlet condition of the specific experiments and assuming an ideal gas. In the CFD simulations, all solid walls were set to the non-slip boundary condition. The conservation equations were solved as a steady-state solution with a segregated solver approach using the SIMPLE algorithm for pressure-velocity coupling. Turbulence is accounted for in the RANS (Reynolds Averaged Navier Stokes) modeling approach, whereas the realizable $k - \varepsilon$ turbulence model with an all y^+ wall treatment was applied.

2.3 Statistical Analysis

Statistical tests were carried out to analyze the void fraction distribution of the synthetically generated packed beds. The Shapiro Wilk test [24, 25] was performed to prove whether the generated void fractions are Gaussian distributed or not. The null hypothesis H_0 of the test is that the investigated sample is drawn from a Gaussian distribution. If the calculated p-value is larger than a chosen threshold level α, H_0 cannot be rejected, and the sample is likely to be Gaussian distributed. For further characterization of non-gaussian distributions, the Pearson moment of skewness is determined, too. A negative moment indicates a left tailed distribution, a positive one a right tailed, whereas an ideal symmetric distribution has a moment of zero. A Kolmogorov-Smirnov test [25] is applied to prove if the experimental and simulated void fractions are drawn from the same distribution. The null hypothesis of this test assumes that the distributions of the two samples are identical. The test fails to reject the null hypothesis, if the p-value is larger than α and the statistic value is smaller than a critical value. The critical value is calculated with the large sample assumption of Smirnov [26].

3 Results

3.1 Void Fraction

The mean void fraction of a given fixed bed depends strongly on the ratio of the reactor-to-particle diameter ratio (D/d_p). In the various correlations of $\varepsilon = f(D/d_p)$ the void fraction is assumed to be a continuous function that decreases with increasing D/d_p. On the other hand, Bufe and Brenner [12] showed the fluctuating nature using the particle rearrangement method for synthetic fixed bed generation. These theoretical results and the experimental data of Seckendorff et al. [1] are shown in Fig. 2.

The comparison of own data with the values of Bufe and Brenner [12] shows similar fluctuations. Nevertheless, the

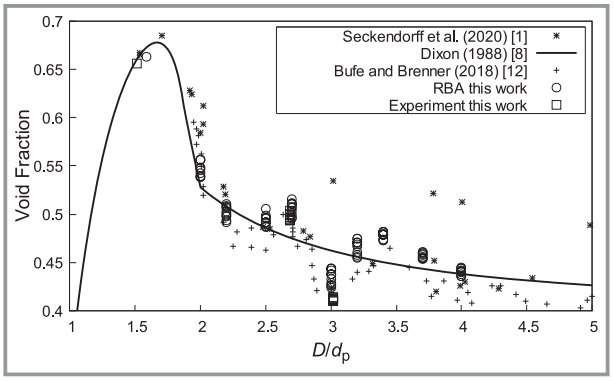

Figure 2. Void fraction of slender fixed beds made from spheres depending on the D/d_p. Experimental data [1], correlation [8], and simulations from literature [12] and own data.

RBA bed structures are more loose (larger void fraction) than the results of Bufe and Brenner [12] This is caused by the particle rearrangement method used in [12], where material properties and the filling method are not taken into account which results in maximum dense beds. However, these factors can have a strong influence on the resulting beds which was demonstrated experimentally by Seckendorff et al. [1]. They authors presented a certain distribution in void fraction for the same D/d_p ratios. The void fraction values in Fig. 2 are very narrowly distributed for $D/d_p < 2$. For these configurations, only one particle per layer can be placed in the tube, which leads to very similar bed structure patterns. Interestingly, we observed very loose bed structures for $D/d_p = 2.68$ and very dense structures for $D/d_p = 3.02$. This finding again agrees with the scatter of [12]. It can be seen that the mean void fraction of the RBA generated bed is located around the values calculated with the equation of Dixon [8]. For this RBA, only ten different variations per D/d_p were generated and plotted in Fig. 2. Since these configurations show a statistical distribution resulting from the randomness of the particle injection, a statistical analysis is required. Using the statistical similarity of synthetic and experimental beds, the fixed bed which best represents the experimentally observed void fraction is chosen for subsequent CFD simulations. This approach is comparable to the method of Jurtz et al. [4] with the difference of a prior statistical analysis of the synthetic and experimental fixed bed void fraction including its distribution.

3.2 Impact of Particle Friction and D/d_p Ratio on the Distribution of the overall Void Fraction

Several authors observed a significant variance between experimentally measured void fractions for the same reactor-to-particle diameter ratio [3, 10]. The variations in ε might origin with decreasing influence from (i) the difference in position from which a particle falls into the tube, (ii) the difference in translational and rotational particle velocity at the start of the fall, (iii) the difference in the time interval between two drops, and (iv) differences in single-particle properties, e.g. diameter, sphericity, and surface roughness. In general, a different bed structure is expected, if different forces act at different times on the bed structure. Moreover, experiments show that the variance in the void fractions might depend on the filling method, the particle material, and the D/d_p ratios [3]. To statistically investigate both the mean value and the distribution of a given void fraction, 100 simulations were carried out each for various friction factors and D/d_p ratios, whereas only the particle position on the injector plane was varied. Fig. 3 shows the cumulative distributions of void fractions for three different D/d_p ratios and Blender friction factors C_{Fric} in a range from 0.1 to 0.9. The mean values, standard deviations, and skewness of the distributions, as well as the results of the Shapiro-Wilk tests, are given in the supporting information.

An increasing friction factor leads to increasing void fractions as reported in [4]. However, the significance of the increased void fraction strongly depends on the actual D/d_p

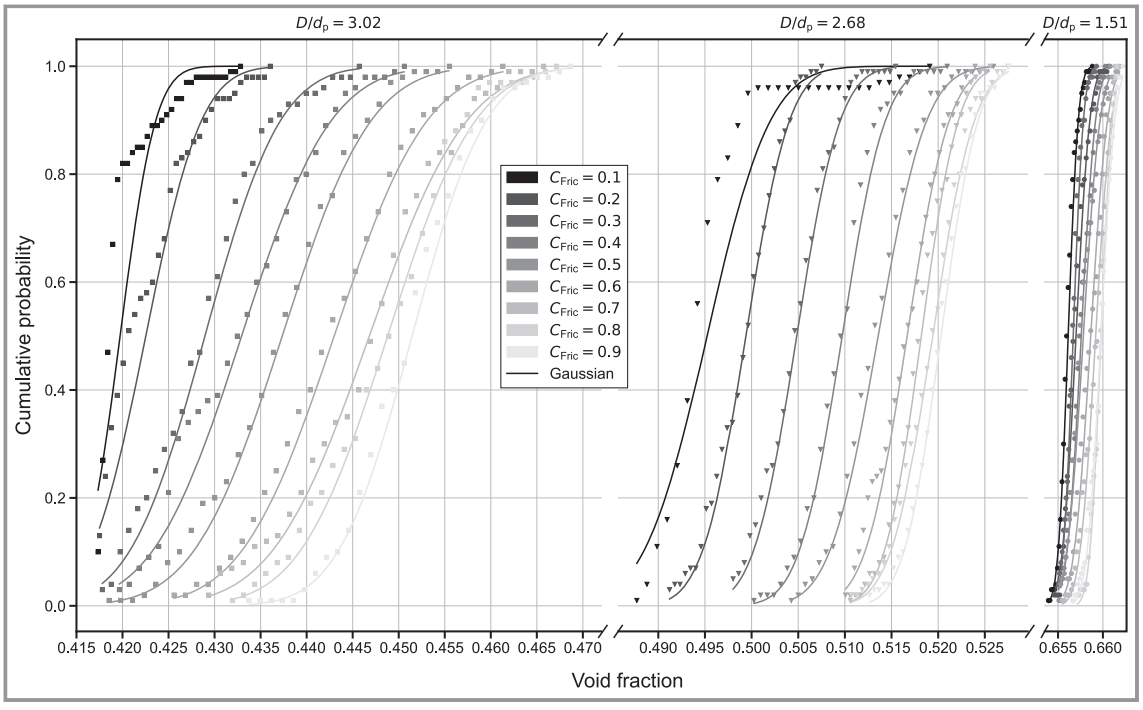

Figure 3. Cumulative distribution of the void fraction for synthetically generated beds made of spheres for three D/d_p ratios and C_{Fric} in a range from 0.1. to 0.9.

ratio. Due to the structuring effect of the tube wall, the friction has only a minor influence for D/d_p = 1.51. This was already suspected in the experimental studies of Seckendorff et al. [1]. Whereas, for D/d_p = 3.02, the spheres can be arranged in a highly structured dense packing. In this case, the friction factor leads to a high impact on the actual packing, because this very dense configuration can be only reached for small frictions. The strong relation between friction factor, structure, and void fraction is shown in Fig. 4, where the particle centroids of one packed bed configuration are plotted for three different friction factors used. With decreasing friction, the order of the bed increases, leading to a highly structured bed for C_{Fric} = 0.001. Of course, this increase in order is leading to lower void fractions.

For D/d_p = 3.02, and for D/d_p = 2.68 high friction factors lead to a symmetric, Gaussian distributed void fraction. However, lower friction factors increase the probability that the particles move into free spaces during the filling process, which leads to non-Gaussian, right tailed distributions, shown in Fig. 3. Due to the already mentioned structuring influence of the wall, this effect does not occur for D/d_p = 1.51, for which the Shapiro Wilk test indicates Gaussian distributed void fractions for all friction factors. Moreover, the standard deviations of the void fractions of packed beds with D/d_p = 1.51 are smaller than those for higher D/d_p ratios. The standard deviations for all D/d_P ratios are in the range determined by Pottbäcker et al. [3]. However, these values are not directly comparable with one another, as different filling methods were used.

In summary, for synthetically generated packed beds, the void fraction significantly depends on the D/d_p ratio and the friction factor, but also on the variance as well as the shape of the void fraction distribution. This should be considered when validating synthetically generated beds with experiments as well as developing correlations based on these beds.

3.3 Experimental Validation of the Synthetically Generated Packed Beds

The packed beds with D/d_p ratios shown in Fig. 3 were also generated experimentally. The filling procedure was repeated ten times. The experimental values are compared via the Kolmogorov-Smirnov test [26] with 100 simulations each for various friction factors. The results of the Kolmogorov-Smirnov test are given in the supporting information.

Tab. 2 lists the experimental mean void fractions and the friction coefficient of the simulations, were the Kolmogorv-Smirnoff test based to reject the null hypothesis. Due to the low impact of C_{Fric} on the void fraction, the experimental data for D/d_p = 1.51 can be described by synthetic packed beds generated with three different friction factors. The configuration D/d_p = 3.02 shows a highly ordered structure, see Fig. 5 for the visual comparison between the experimentally and synthetically generated bed. In the RBA the particles can move into a highly ordered structure when the friction forces acting on the particles are small. Therefore,

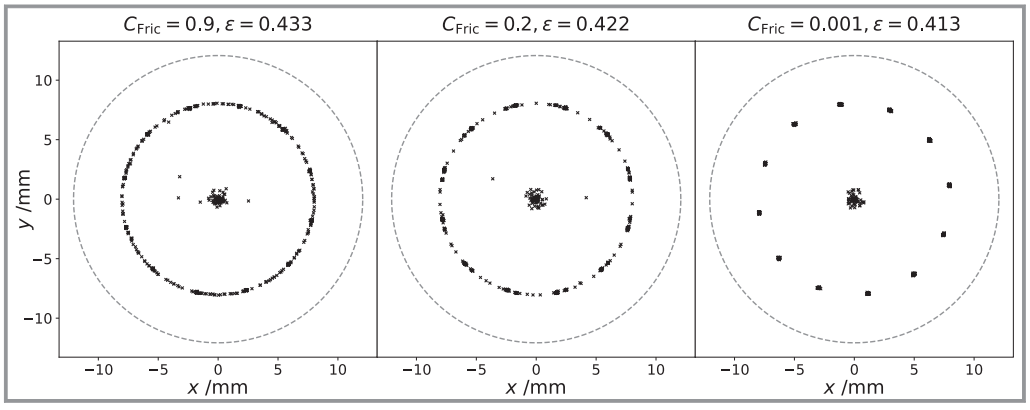

Figure 4. Centroids of the spheres with D/d_p = 3.02 in a 600 mm high packed bed for various C_{Fric}.

Table 2. Experimental void fraction and friction coefficient for Kolmogorov-Smirnov *p*-value > α, using a tube diameter *D* of 24.14 mm.

d_p [mm]	(D/d_p)	Material	Mean ε [–]	Standard deviation [%]	$C_{Fric,p>\alpha}$ [–]
16	1.51	Steel	0.656	0.088	0.1, 0.2, 0.3
9	2.68	Glass	0.498	0.618	0.1, 0.2
8	3.02	Glass	0.412	0.333	0.001

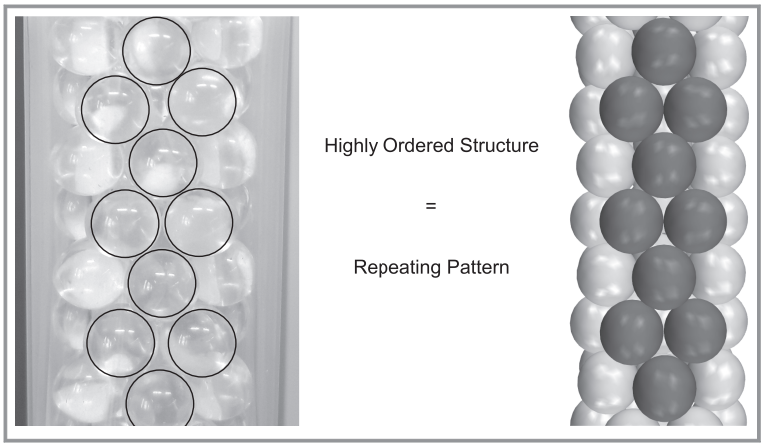

Figure 5. Highly ordered structure observed for the experimentally and synthetically generated packed beds for $D/d_p = 3.02$.

only a very low friction factor can reflect the experimental dense structure. Such extreme values for the friction factor are only needed to generate highly ordered packed beds.

Tab. 2 shows that the friction is significantly higher for glass and steel particles for the other two bed configurations. Both materials show very smooth surfaces. Thus, $D/d_p = 3.02$ can be interpreted as a special case, since the preferred state of the bed is a highly ordered structure. Due to the limited number of experiments, it is unclear who the exact void fraction distributions look like.

3.4 Effect of Local Bed Structure on the Flow Field

In the following, different D/d_p configurations of fixed beds are simulated with CFD and the results are compared with typical pressure drop correlations as well as measured values. The velocity is represented as the relative velocity v_{Rel}, using the superficial velocity v_0 and the velocity magnitude $|\mathbf{v}|$.

$$v_{Rel} = \frac{|\mathbf{v}|}{v_0} \tag{6}$$

The pressure drop is plotted against the modified particle Reynolds number Re_p^*, calculated with the mean void fraction ε.

$$Re_p = \frac{d_p \rho v_0}{\mu} \tag{7}$$

$$Re_p^* = \frac{Re_p}{1-\varepsilon} \tag{8}$$

By using the modified particle Reynolds number Re_p^*, the deviations in pressure drop caused by differences in void fraction are compensated and the values become more comparable. In Fig. 6 the pressure drop of the simulations and the Ergun as well as the Eisfeld-Schnitzlein equation is shown [14, 15]. As can be seen in Fig. 6a, the particle resolved CFD simulation of the $D/d_p = 1.51$ reproduces the experimental pressure drop. A comparison with the Eisfeld-Schnitzlein equation for this configuration is however not possible, because the correlation is not valid for $D/d_p < 1.624$. The Ergun equation overpredicts the experimental pressure drop by approx. 30 % for the highest Re_p^*. For the configuration of $D/d_p = 2.68$, a channel was observed in the bed center. This explains the high void fraction found for this bed (cf. Fig. 2) as well as the overprediction of the pressure drop by the Eisfeld-Schnitzlein equation (Fig. 6 b) and even more severe the Ergun equation. Since these correlations do not account for the actual local bed structure, the pressure drop is predicted higher than the measured and simulated one. The channel that forms in the bed center is a region of low flow resistance and therefore leads to a total lower pressure drop. For the $D/d_p = 3.02$, the bed structure is rather dense (cf. Figs. 4 and 5). The wall channel effect is very pronounced in this case, because the highly ordered structure has 6 particles placed close to the wall while only 1 particle is in the center of the bed (Fig. 4). This leads to an additional small channeling effect, by the formation of an annular gap around the centered particles. Since the Eisfeld-Schnitzlein equation again cannot consider this local arrangement, the pressure drop is calculated too high. Again, the CFD simulation shows a good agreement with the measured pressure drop values (Fig. 6c).

The configuration of $D/d_p = 2.68$ shows a channel in the center of the synthetic packed bed through which the fluid can pass without a barrier (Fig. 6b). The formation of a channel through the bed is in line with the investigation of Guo et al. [27]. They also observed a channel for a comparable D/d_p of 2.73. This formation of a channel is not characteristic for the synthetic bed only, it was also observed for the experimental bed with $D/d_p = 2.68$ (Fig. 7).

In Addition to the configurations where a channel was observed, simulations were carried out for fixed beds without these effects. For $D/d_p = 2$, the CFD simulation agrees with the Eisfeld-Schnitzlein correlation (Fig. 8a). A small change in dimensions from $D/d_p = 2.68$ (Fig. 6b) to $D/d_p = 2.7$ (Fig. 8b) results in a closure of the channel. In this rather randomized particle arrangement, the fluid cannot take any direct path, which leads to an agreement between the CFD simulation and the Eisfeld-Schnitzlein correlation, while the Ergun equation tends to a small overestimation.

This comparison of different beds made of spheres proves that the local bed structure has a large influence on the actual pressure drop, which is for some configurations not captured by the Eisfeld-Schnitzlein and Ergun correlation.

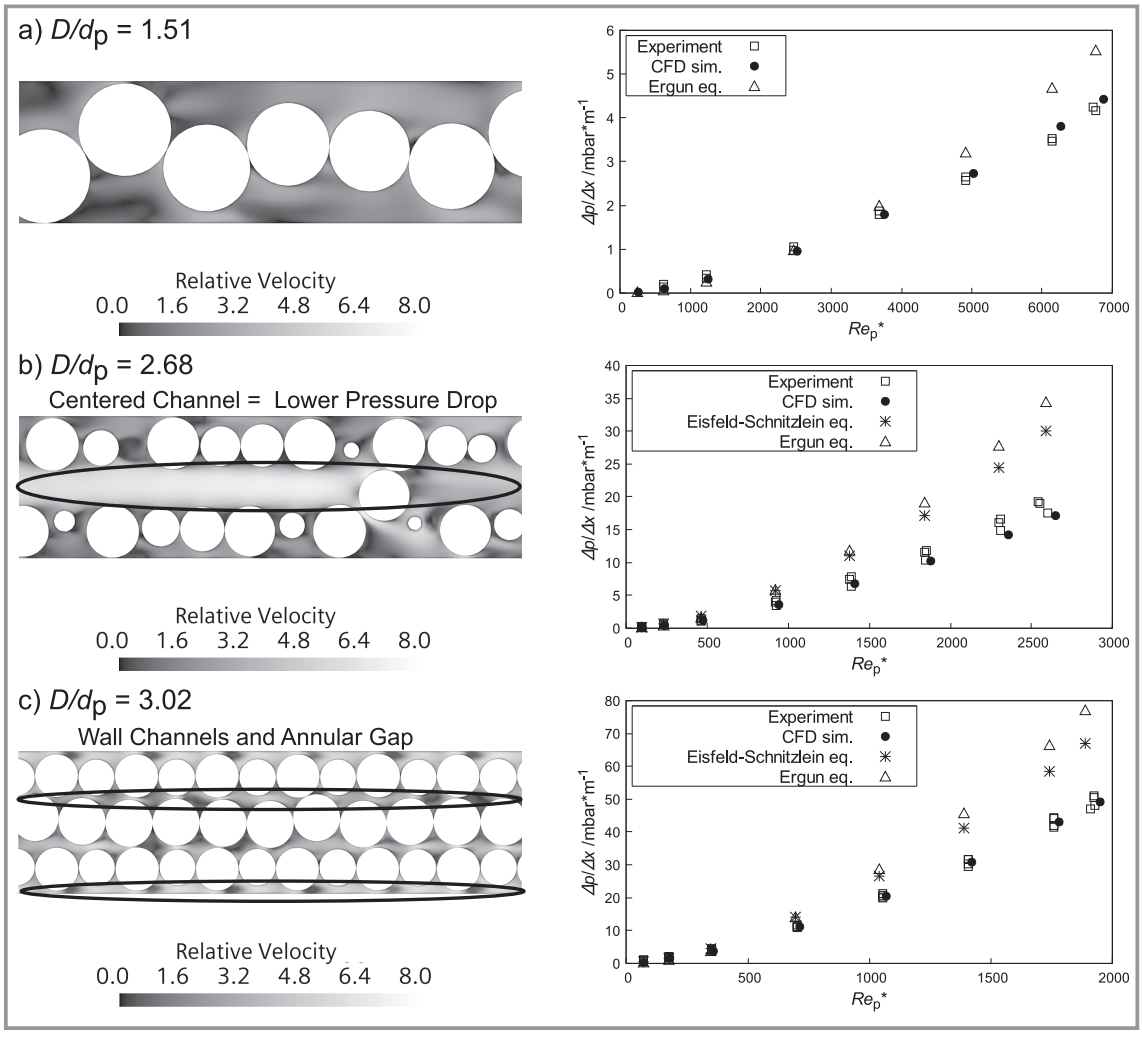

Figure 6. Channeling effect in fixed beds for different D/d_p. Velocity scenes through the bed and comparison of pressure drop correlations with experimental data and CFD simulations.

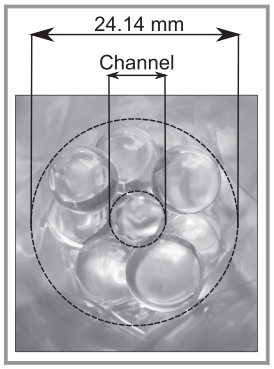

Figure 7. Channel building in an experimental fixed bed of D/d_p = 2.68.

For slender fixed beds, the formation of channels is possible, which reduces the pressure drop over the bed length. While the Eisfeld-Schnitzlein equation can be used to predict the pressure drop in a bed with a rather random structure, strong deviations occur for configurations with local structural effects, i.e. centered or annular channels, pockets, etc.

4 Conclusion

We showed that the void fraction of synthetically generated packed beds are statistically distributed. The shapes of these distributions depend on the D/d_p ratio as well as on the friction factor used in the model. For D/d_p ratios with dominating, structuring wall effects, the void fractions are normally distributed, whereas larger D/d_p ratios form right tailed distributions for small friction factors. While various factors can influence the distribution (e.g., filling method, filling rate, restitution coefficient, etc.), we have concentrated on the friction factor in this study. This allows us to adapt the synthetically generated fixed beds to the experimental beds using statistical tests. CFD simulations were carried out with representative beds and compared with experiments. The combined results showed that the pressure drop of an actual bed configuration is a complex issue that does not only depend on the average void fraction. Void fraction and

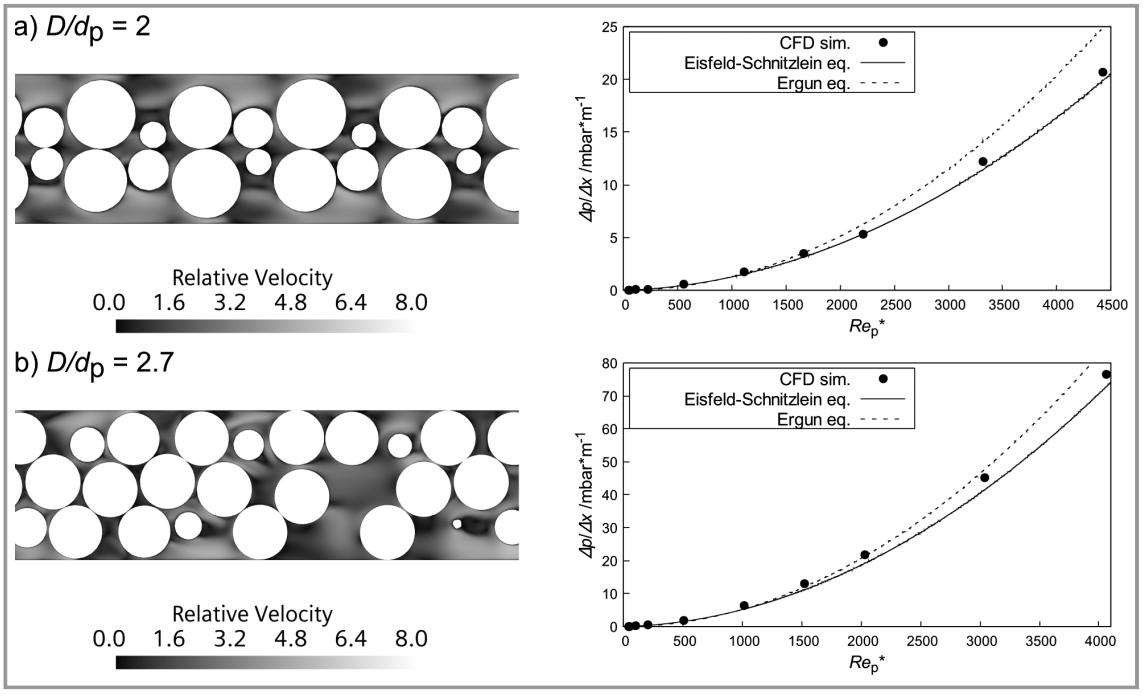

Figure 8. Pressure drop in fixed beds without a channel for different D/d_p. Velocity scenes through the bed and comparison of pressure drop correlations with the CFD simulations.

pressure drop correlations fail for some configurations, because they only depend on the mean void fraction and do not account for local bed structures that might form channels or annular gaps. These open spaces with a low flow resistance lead to an overestimation of pressure drop when applying typical correlations. The description of the pressure drop by empirical equations leads only to sufficient agreements, if the flow paths through the bed are deflected and not channeled. On the other hand, particle-resolved CFD simulations can reproduce the experimental results, since they are based on three-dimensional bed structures.

The investigation in this work focused on the pressure drop as a quantity based on fluid dynamics. Other important properties of fixed bed reactors, which are affected by fluid dynamics, are heat and mass transport and local reaction rates. While the simulated pressure drop is in agreement with the experimental values, these other important phenomena need further validation cases. In future research, the statistical analysis will be extended to more complex particle shapes and different filling methods.

Supporting Information

Supporting Information for this article can be found under DOI: https://doi.org/10.1002/cite.202000171.

This publication is based upon work supported and financed by Clausthal University of Technology, project Catalytic and microbial methanation as basis for sustainable energy storage (CliMb). Open access funding enabled and organized by Projekt DEAL.

Symbols used

D	[m]	reactor diameter
$\mathbf{D}$	[s^{-1}]	deformation tensor
d_p	[m]	particle diameter
C	[–]	RBA property coefficient
H	[m]	filling height
H_0	[–]	null hypothesis
$\mathbf{I}$	[–]	unit tensor
N	[–]	particle count
p	[Pa]	pressure
p	[–]	p-value
Re_p	[–]	particle Reynolds Number $Re_p = \frac{d_p \rho v_0}{\mu}$
$Re_p{}^*$	[–]	modified particle Reynolds number $Re_p{}^* = \frac{Re_p}{1-\varepsilon}$
$\mathbf{T}$	[Pa]	stress tensor
v_0	[m s^{-1}]	superficial velocity

v_{Rel}	[–]	relative velocity
$\mathbf{v}$	[m s^{-1}]	velocity vector

Greek letters

α	[–]	significance value
ε	[–]	void fraction
μ	[Pa s]	viscosity
ρ	[kg m^{-3}]	density

Sub- and superscripts

dense	fixed bed with the dense configuration
Fric	friction coefficient
loose	fixed bed with the loose configuration
Res	restitution coefficient

Abbreviations

CAD	computer-aided design
CFD	computational fluid dynamics
DEM	discrete element method
RANS	Reynolds averaged Navier Stokes
RBA	rigid body approach
SIMPLE	semi-implicit method for pressure linked equations

References

[1] J. von Seckendorff, N. Szesni, R. Fischer, O. Hinrichsen, *Chem. Eng. Sci.* **2020**, *222*, 115644. DOI: https://doi.org/10.1016/j.ces.2020.115644

[2] J. Fernengel, J. von Seckendorff, O. Hinrichsen, *Comput. Aided Chem. Eng.* **2018**, *43*, 97–102. DOI: https://doi.org/10.1016/B978-0-444-64235-6.50019-X

[3] J. Pottbäcker, O. Hinrichsen, *Chem. Ing. Tech.* **2017**, *89 (4)*, 454–458. DOI: https://doi.org/10.1002/cite.201600151

[4] N. Jurtz, P. Waldherr, M. Kraume, *Chem. Ing. Tech.* **2019**, *66 (5)*, 705. DOI: https://doi.org/10.1002/cite.201800190

[5] L. H. S. Roblee, R. M. Baird, J. W. Tierney, *AIChE J.* **1958**, *4 (4)*, 460–464. DOI: https://doi.org/10.1002/aic.690040415

[6] M. Giese, K. Rottschäfer, D. Vortmeyer, *AIChE J.* **1998**, *44 (2)*, 484–490. DOI: https://doi.org/10.1002/aic.690440225

[7] R. Jeschar, *Arch. Eisenhüttenwes.* **1964**, *35 (2)*, 91–108. DOI: https://doi.org/10.1002/srin.196402300

[8] A. G. Dixon, *Can. J. Chem. Eng.* **1988**, *66 (5)*, 705–708. DOI: https://doi.org/10.1002/cjce.5450660501

[9] E. A. Foumeny, H. A. Moallemi, C. Mcgreavy, J. A. A. Castro, *Can. J. Chem. Eng.* **1991**, *69 (4)*, 1010–1015. DOI: https://doi.org/10.1002/cjce.5450690425

[10] F. Benyahia, K. E. O'Neill, *Part. Sci. Technol.* **2005**, *23 (2)*, 169–177. DOI: https://doi.org/10.1080/02726350590922242

[11] V. M. H. Govindarao, K. V. S. Ramrao, A. V. S. Rao, *Chem. Eng. Sci.* **1992**, *47 (8)*, 2105–2109. DOI: https://doi.org/10.1016/0009-2509(92)80330-F

[12] A. Bufe, G. Brenner, *Transp. Porous Media* **2018**, *123 (2)*, 307–319. DOI: https://doi.org/10.1007/s11242-018-1043-0

[13] E. Erdim, Ö. Akgiray, I. Demir, *Powder Technol.* **2015**, *283*, 488–504. DOI: https://doi.org/10.1016/j.powtec.2015.06.017

[14] S. Ergun, *Chem. Eng. Prog.* **1952**, *48*, 89–94.

[15] B. Eisfeld, K. Schnitzlein, *Chem. Eng. Sci.* **2001**, *56 (14)*, 4321–4329. DOI: https://doi.org/10.1016/S0009-2509(00)00533-9

[16] A. G. Dixon, M. Nijemeisland, *Ind. Eng. Chem. Res.* **2001**, *40 (23)*, 5246–5254. DOI: https://doi.org/10.1021/ie001035a

[17] N. Jurtz, M. Kraume, G. D. Wehinger, *Rev. Chem. Eng.* **2019**, *35 (2)*, 139–190. DOI: https://doi.org/10.1515/revce-2017-0059

[18] B. Partopour, A. G. Dixon, *Powder Technol.* **2017**, *322*, 258–272. DOI: https://doi.org/10.1016/j.powtec.2017.09.009

[19] S. Flaischlen, G. D. Wehinger, *ChemEngineering* **2019**, *3 (2)*, 52. DOI: https://doi.org/10.3390/chemengineering3020052

[20] E. M. Moghaddam, E. A. Foumeny, A. I. Stankiewicz, J. T. Padding, *Ind. Eng. Chem. Res.* **2018**, *57 (44)*, 14988–15007. DOI: https://doi.org/10.1021/acs.iecr.8b03915

[21] J. Bender, K. Erleben, J. Trinkle, *Comput. Graphics Forum* **2014**, *33 (1)*, 246–270. DOI: https://doi.org/10.1111/cgf.12272

[22] T. Eppinger, K. Seidler, M. Kraume, *Chem. Eng. J.* **2011**, *166 (1)*, 324–331. DOI: https://doi.org/10.1016/j.cej.2010.10.053

[23] G. D. Wehinger, C. Fütterer, M. Kraume, *Ind. Eng. Chem. Res.* **2017**, *56 (1)*, 87–99. DOI: https://doi.org/10.1021/acs.iecr.6b03596

[24] P. Royston, *Appl. Stat.* **1995**, *44 (4)*, 547. DOI: https://doi.org/10.2307/2986146

[25] N. M. Razali, Y. B. Wah, *J. Stat. Model. Anal.* **2011**, *2 (1)*, 21–33.

[26] J. L. Hodges, *Arkiv Matematik* **1958**, *3 (5)*, 469–486. DOI: https://doi.org/10.1007/BF02589501

[27] Z. Guo, Z. Sun, N. Zhang, M. Ding, J. Wen, *Chem. Eng. Sci.* **2017**, *173*, 578–587. DOI: https://doi.org/10.1016/j.ces.2017.08.022

